JOURNAL OF CATALYSIS 114, 153–166 (1988)

Studies of Skeletal Rearrangements of Labeled Hexanes on Iridium and Iridium–Cobalt Catalysts: Correlations between the Product Distributions and Some Structural Information on the Catalysts Given by EXAFS

P. ESTEBAN PUGES,* F. GARIN,* F. WEISANG,† P. BERNHARDT,* P. GIRARD,* G. MAIRE,*,[1] L. GUCZI,‡ AND Z. SCHAY‡

*Laboratoire de Catalyse et Chimie des Surfaces, U.A. 423 du CNRS, Institut Le Bel, Université Louis Pasteur, 4 rue Blaise Pascal, 67070 Strasbourg, France; †L'Air Liquide, rue Michaël Faraday, 78390 Bois d'Arcy, France; and ‡Institute of Isotopes of the Hungarian Academy of Sciences, P.O. Box 77, H-1525 Budapest, Hungary

Received December 24, 1987

Isomerization of hydrocarbons using ^{13}C-labeled molecules over both iridium and iridium–cobalt catalysts proceeds via a selective cyclic mechanism. By decreasing the iridium loading from 10 to 0.25 wt% or by adding cobalt to iridium, isomerization via bond-shift intermediates becomes more important. For C–C bond rupture a methyl migration mechanism is favored, whereas the tertiary carbon atom always seems to be nonreactive. To explain the change in the reaction pathway, an alkyne mechanism was postulated in which the alkyne species are in equilibrium with the surface carbynes. The former species are favored when adsorbed hydrogen is less available, which is the case with cobalt as seen by TPR measurements on bimetallic cobalt–iridium catalysts. On the other hand, carbynes are the precursor species for the selective cyclic mechanism or for selective demethylation. The catalytic results are well supported by EXAFS measurements. The multiple scission of the C–C bonds characteristic of cobalt is suppressed by the presence in the topmost layer of iridium atoms surrounded by cobalt atoms. Total surface iridium concentration is constant irrespective of the iridium loading as also seen by TPR measurements. From EXAFS data, it is shown that iridium atoms (i) are involved in a bimetallic phase very diluted in iridium having a unit mesh identical to that of hexagonal cobalt; (ii) are involved in very small aggregates of iridium embedded in the matrix of cobalt with iridium–iridium distances of 0.265 nm (these aggregates are insensitive to oxidation passivated by cobalt and then catalytically inactive); and (iii) are in some cases making large fcc particles of iridium, particularly when the catalyst is heated at 1273 K in helium. The catalytic results are discussed via two hypotheses: (i) an electronic interaction between iridium and cobalt and (ii) the availability of surface hydrogen. Both hypotheses are directly correlated to the product distribution observed during the surface rearrangement.

INTRODUCTION

Skeletal rearrangement of hydrocarbons on iridium catalysts takes place mainly via a selective C_5-cyclic type mechanism and marginally by a bond-shift mechanism (*1*). Interconversion between 2-methylpentane and 3-methylpentane can be interpreted by the selective cyclic mechanism, whereas *n*-hexane never participates in the cyclic reaction. Hydrogenolysis of methylcyclopentane is also selective because the ratio of 3-methylpentane to *n*-hexane amounts to about 20 (*2*). Hydrogenolysis of cyclic alkanes on iridium catalysts revealed that mainly the rupture of secondary–secondary or secondary–primary carbon–carbon bonds is favored. Such a characteristic behavior of Ir/Al_2O_3 catalysts seems to be largely independent of dispersion and of the method of preparation (*1*). For example, a 0.25 wt% Ir/Al_2O_3 catalyst derived from

[1] To whom all correspondence should be addressed.

0021-9517/88 $3.00

$Ir_4(CO)_{12}$ leads to the same selectivity in both hydrogenolysis (acyclic or cyclic) and isomerization as the classical 10 wt% Ir/Al_2O_3 sample (*3*).

In contrast to iridium, on Pt/Al_2O_3 the selectivity pattern, i.e., the relative contribution of isomerization to hydrogenolysis, changes with platinum dispersion (*4*). Although cobalt is considered to be an extensive cracking catalyst, its addition to platinum never results in enhanced cracking activity but simply in a shift toward formation of intermediates by bond shift (*5, 6*). The platinum–cobalt ensembles do not exhibit the intrinsic isomerization and cracking activities that are characteristic of platinum and of cobalt, respectively, and this can be interpreted by a strong cobalt–platinum interaction.

In the present work EXAFS experiments have been carried out with the aim of obtaining better information about the structure of Co–Ir bimetallic catalysts in addition to what has been gathered in TPR and hydrogen TPD studies (*7*). We also wish to look for correlations between the catalyst structure and the selectivity pattern displayed in hydrocarbon transformations. For a better understanding ^{13}C-labeled hydrocarbons are applied.

EXPERIMENTAL

Catalysts

Catalysts were prepared by coimpregnation or successive impregnations on Al_2O_3 manufactured by Woelm A.G. (154 m^2/g, 0.28 cm^3/g pore volume). Chemical-grade $H_2IrCl_6 \cdot 6H_2O$ and $Co(NO_3)_2 \cdot 6H_2O$ were purchased from Johnson Matthey and Merck, respectively.

Catalysts prepared by coimpregnation. Atomic and weight compositions of the samples are listed in Table 1. The total proportion of metals (iridium + cobalt) is always 10%. Prior to the reaction, catalysts were reduced *in situ* in a stream of H_2 at 973 K for 6 h. Catalyst B* signifies catalyst B treated at 1273 K under helium for 6 h.

TABLE 1

Atomic and Weight Percentages for Various Co_xIr_{x-1}/Al_2O_3 Catalysts

Atomic composition					Percentage in weight				Preparation
A			Ir	100			Ir	10.0	
B*[a]	Co	49	Ir	51	Co	2.3	Ir	7.7	Coimpregnation
C	Co	68	Ir	32	Co	4.0	Ir	6.0	Coimpregnation
D	Co	84.8	Ir	15.2	Co	6.1	Ir	3.9	Coimpregnation
E	Co	93.3	Ir	6.7	Co	8.1	Ir	1.9	Coimpregnation
F	Co	97.8	Ir	2.2	Co	9.3	Ir	0.7	Coimpregnation
G	Co	99	Ir	1	Co	9.7	Ir	0.3	Coimpregnation
H	Co	100			Co	10.0			
I(a,b)	Co	98	Ir	2	Co	9.3	Ir	0.7	Successive
J(a,b)	Co	84	Ir	16	Co	6.1	Ir	3.9	impregnations

[a] B* = catalyst B treated at 1273 K under helium (6 h).

Catalysts prepared by successive impregnations. Some catalysts—Ia, Ib, Ja, Jb (Table 1)—were prepared by successive impregnations as follows:

For Ia and Ja, the Al_2O_3 carrier was first impregnated with a solution of $H_2IrCl_6 \cdot 6H_2O$, then calcined in air at 673 K and reimpregnated with an aqueous solution of $Co(NO_3)_2$ followed by calcination in air at 673 K.

For Ib and Jb, the inverse procedure of impregnation was applied, i.e., cobalt salt was deposited first. The calcination steps were the same as for Ia and Ja.

The catalysts were heated in a stream of hydrogen at 653 K for 14 h.

Hydrocarbons

All ^{13}C-labeled hydrocarbons were prepared from the corresponding labeled alcohols. The synthesis of these compounds has been described previously (*8*). The starting labeled materials were obtained from Merck Sharpe and Dohme (Canada).

Catalytic Tests

Catalytic reactions were carried out in the all-glass, grease-free flow system already described (*9*). Reactions were performed at atmospheric pressure with a partial pressure H_2-to-hydrocarbon ratio of 120.

EXAFS Measurements

The procedure for EXAFS measurements has been described elsewhere (*10*). The synchrotron radiation was that produced in the DCI storage ring of LURE (Orsay) running at 1.72 GeV, with an average current of 200 mA. The monochromator used was a channel-cut Si(311) crystal, the signal being extracted through two ion chambers. Cells about 1 mm thick, with sealed Kapton windows, were used as sample holders. EXAFS spectra were recorded above the iridium L_{III} edge (11,215 eV) and the cobalt K edge (7709 eV) for catalysts B*, C, D, F, and G after reduction in Strasbourg and transfer to LURE in an argon atmosphere. EXAFS spectra were obtained from the absorption spectra in a conventional manner by subtracting a Victoreen fit in the pre-edge region. Fourier transform technique was used to isolate the EXAFS contribution due to the first coordination shell. A curve-fitting technique was applied to determine the values of the "EXAFS parameters." Fitting was accomplished by means of an iterative least-squares procedure (*11*). The λ parameter (mean free path of photoelectron) was introduced for a photoelectron energy of 200 eV and then extrapolated for the other values of E with the expression $\lambda = CE^{-2}$. By using the amplitude and phase functions calculated by Teo and Lee (*12*), it was possible on iridium and cobalt foils and on 10 wt% Co/Al_2O_3 and 10 wt% Ir/Al_2O_3 catalysts to fit the experimental EXAFS oscillations until the fifth coordination shell, for example in the case of iridium (*28*). Although the parameters for amplitude and phase functions were not extracted from well-defined iridium and cobalt compounds, the errors in the distances were less than 0.03 Å.

RESULTS

EXAFS Results

In Table 2 are the results obtained by analyzing EXAFS oscillations beyond both the L_{III} edge of iridium and the K edge of cobalt for catalysts B*, C, F, and G (see Table 1). The first neighborhood contribution was isolated in every case by inverse Fourier transformation over a limited range of R (radius). The curve-fitting technique was then applied to determine the EXAFS parameters.

Figures 1a and b show, respectively, the modulus of the k^3-weighted EXAFS experi-

TABLE 2

Structural Parameters of Alumina-Supported Co_xIr_{1-x} Catalysts Derived from EXAFS Data

Catalysts	Absorption edge	Number of nearest neighbors			Distance (Å)			
		Co	Ir	O	Co–Co	Co–Ir	Ir–Ir	Co–O
B*[a] $Co_{49}Ir_{51}$	Ir		12		—	—	2.72	—
C	Co	10.6	—	2.2	2.50	—	—	1.93
$Co_{68}Ir_{32}$	Ir	2.0	8.6		—	2.49	2.65	—
F	Co	8.5	—	2.0	2.49	—	—	1.90
$Co_{97.8}Ir_{2.2}$	Ir	3	2.2	—	—	2.50	2.65	—
G	Co	1.8	—	1.3	2.50	—	—	1.93
$Co_{99}Ir_1$	Ir	3.7	—	—	—	2.49	—	—

[a] B* = catalyst B treated at 1273 K under helium (6 h).

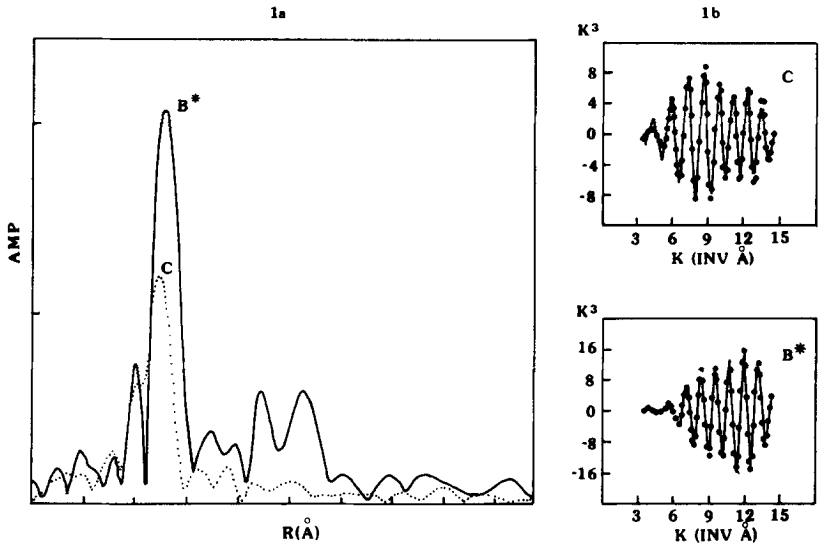

FIG. 1. (a) Modulus of the Fourier-transformed k^3-weighted EXAFS experimental data obtained from the Ir L_{III} edge for samples B* and C. Hanning window ranges from 40 to 140 nm^{-1} in k space. (b) Superposition of the k^3-weighted EXAFS oscillations: (—) For samples B* and C from the inverse Fourier transform ranging from 0.18 to 0.32 nm in phase space. (●) Calculated with the corresponding parameters indicated in Table 2.

mental data obtained from the L_{III} Ir edge for samples B* and C, applying a Hanning window between 40 and 140 nm^{-1}, and the superposition of the k^3-weighted EXAFS oscillations obtained from the inverse Fourier transform, ranging from 0.18 to 0.32 nm in phase space, and of the fit with the corresponding parameters indicated in Table 2. In Fig. 2a, the modulus of the Fourier-transformed k-weighted EXAFS experimental data is given for samples C and F. In Fig. 2b, the k-weighted Fourier-transformed fits corresponding to the EXAFS oscillations on the K edge of Co, with the Hanning window ranging from 40 to 130 nm^{-1}, are presented for samples C and F. EXAFS parameters obtained for the first shell on iridium L_{III} and cobalt K edges are reported in Table 2 for catalysts B*, C, F, and G. In sample B* only one Ir–Ir distance (0.272 nm) for the iridium surrounded by 12 near neighbors in the first coordination shell can be found. The Fourier transform for catalyst B* is exactly the same as that for an iridium foil. The EXAFS oscillations are fitted by fcc iridium until the third coordination shell. By X-ray diffraction large particles of iridium ($d > 10$ nm) were identified. The formation of these large iridium particles was attributed to sintering during the heating to 1273 K under helium. The catalytic properties of sample B* agree with those of a classical Ir/Al_2O_3 catalyst (see Catalytic Results).

The following observations were made for catalysts C, D, F, and G:

- The Fourier transforms for catalysts C, D, F, and G treated at 700°C are different from that for catalyst B*. Beyond the absorption edge of iridium the Fourier transform is more intense for catalyst B* (see Fig. 1a for comparison between catalysts B* and C) and the main peak is shifted to lower distances.
- There is a surprisingly short Ir–Ir distance of 0.265 nm for samples C, D, and F but without any Ir–Co distance at 0.265 nm.

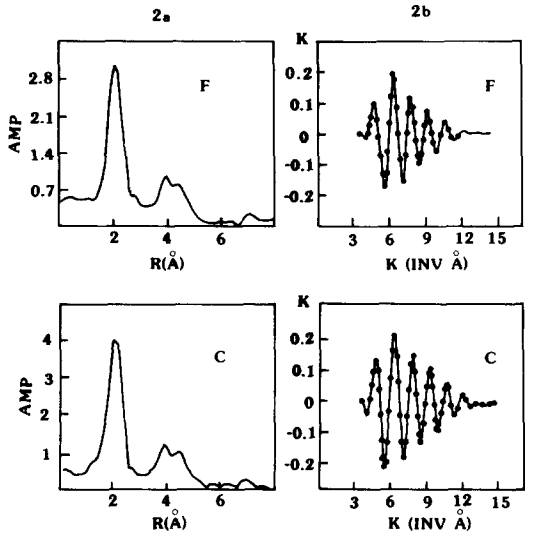

FIG. 2. (a) Modulus of the Fourier-transformed k-weighted EXAFS experimental data obtained from the Co K edge for samples C and F. (b) Superposition of the k^3-weighted EXAFS oscillations: (—) For samples C and F from the inverse Fourier transform ranging from 0.07 to 0.3 nm in the phase space. (●) Calculated with the corresponding parameters indicated in Table 2.

- Co–Co and Co–Ir distances of 0.250 nm are present for samples C, F, and G but the Co–Ir distance was deduced only from the EXAFS data on the absorption edge of iridium and never on the absorption edge of cobalt.
- Specifically on the absorption edge of cobalt, there are Co–O distances around 0.192 nm on all samples due to some contamination by air.
- No Co–Ir distances at 0.250 nm exist as deduced from EXAFS beyond the cobalt K edge.
- For sample D there is an Ir–Ir distance of 0.272 nm identical to the observation on sample B* which is attributable to the presence of a separate phase of iridium on the support.

Analysis of the EXAFS data, although not obtained during *in situ* experiments, led us to make the following comments: (a) Catalyst B* treated under He at 1273 K comprises large fcc Ir particles. No EXAFS measurements were taken on the Co K edge, the catalytic properties being those of a classical 10% Ir/Al_2O_3 (*1*). X-ray diffraction showed superimposition of Ir crystallites and of cobalt aluminate (*29*). (b) At first glance, for catalysts C, D, and F, the presence of short Ir–Ir distances (0.265 nm) may be thought of as an indication of the existence of Ir_xCo_{1-x} alloy. In such a case bimetallic particles with Ir–Co distances identical with Ir–Ir bond length should also be present: using a nonlinear least-squares refinement, no Ir–Co distances with 0.265 nm can be introduced without having the goodness of the fits (on both Ir L_{III} and Co K edges) seriously violated. This leads us to discard the hypothesis of the existence of an Ir_xCo_{1-x} alloy and to focus on the existence of the short Ir–Ir distances (0.265 nm) to monometallic iridium clusters embedded in the cobalt matrix. This hypothesis is favored by three arguments:

1. These Ir contracted clusters are not sensitive to oxidation in air and are inactive in catalysis.
2. Whatever the concentration of Ir in the catalyst the catalytic results seem to correlate to a constant composition of iridium in the topmost layer as seen also by TPR measurements (*7*).
3. Recent *in situ* experiments under hydrogen confirm completely the EXAFS data described here (*30*) (Ir–Ir distances at 0.265 nm and Ir–Co distances at 0.249 nm) and show that for coimpregnated Ir–Co catalysts, chloroiridic acid is first adsorbed on alumina and iridium atoms, and clusters after calcination and reduction diffuse into the matrix of Co, the reduction of iridium occurring simultaneously with that for cobalt. The existence of Ir–Co distances at 0.249 nm on catalysts C, F, and G beyond the iridium L_{III} edge but not beyond the cobalt K edge is explained by the presence of atomic iridium surrounded by cobalt atoms in the topmost layer. As the number of Co–Co distances is much higher than the number of Co–Ir distances, these Co–Ir dis-

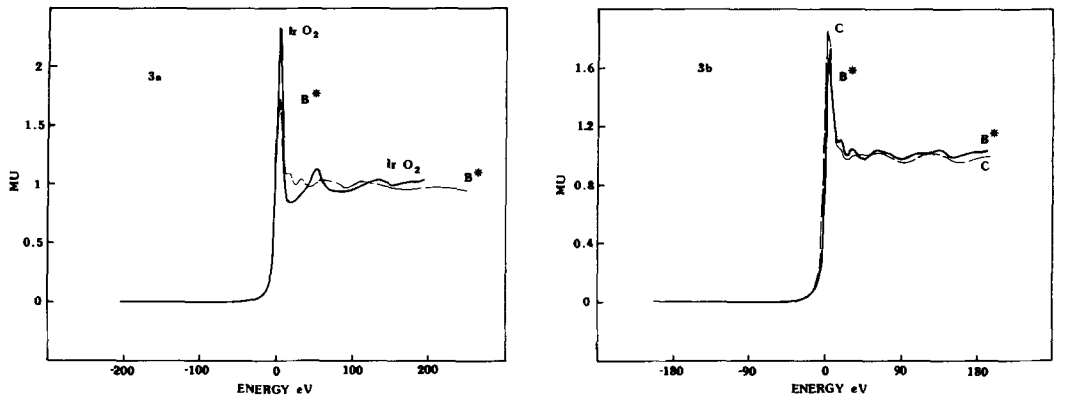

FIG. 3. (a) Normalized NEXAFS (L_{III} edge of iridium) for iridium oxide (—) and catalyst B* (---). (b) Normalized NEXAFS (L_{III} edge of iridium) for catalysts B* (—) and C (---).

tances are not detected in the analysis of the measurements on the cobalt K edge.

NEXAFS on the L_{III} edge of iridium. The presence of metallic particles of iridium even after contamination by air as deduced from EXAFS analysis on the L_{III} edge of iridium is confirmed by the structure observed near the L_{III} edge. Figures 3a and b represent the structures near the absorption edge of iridium for an iridium oxide reference for catalysts B and C. In Fig. 3a the NEXAFS for the reference iridium oxide is compared with that for catalyst B which is characteristic of metallic iridium (*15, 28*). The iridium spectrum beyond the absorption edge is more complex than the iridium oxide spectrum, the white line being more intense in the case of iridium oxide. In Fig. 3b the NEXAFS for catalysts B and C are compared. For both catalysts the intensity of the white line is similar. In contrast with the oxide case, the features observed beyond the absorption edge in catalyst C closely follow those observed in the case of B*, even if they are softened due to a smaller cluster size. This is in full agreement with the conclusions drawn from EXAFS data.

In conclusion we deduce that three types of iridium atoms contribute to these catalysts studied by EXAFS: (i) iridium atoms in large crystallites of iridium (Ir–Ir = 0.272 nm); (ii) iridium atoms in small contracted clusters embedded in the cobalt matrix (Ir–Ir = 0.265 nm) unreactive on exposure to air or during the catalytic test; (iii) iridium atoms in the topmost layer surrounded by cobalt atoms (Ir–Co = 0.249 nm).

Catalytic Results

Catalytic behavior of iridium catalysts. Before the iridium–cobalt bimetallic catalyst was studied, pure iridium catalysts with different metal loadings were investigated in the catalytic conversion of 2-methylpentane. The results are presented in Table 3. As shown here the total activity measured at 493 K is high, whereas the selectivity for isomerization is rather low.

The cracking pattern very clearly shows that deethylation reactions are favored over demethylation reactions and that the $(C_2 + C_4)/(C_1 + C_5)$ ratio increases from 1.3 to 2.5 when the amount of iridium decreases from 10 to 0.25 wt%. The internal C–C bond fission leading to propane is of minor importance, as rupture of carbon–carbon bonds involving a tertiary carbon atom is not favored. This remark can be generalized to the various demethylation reactions leading preferentially to isopentane formation. The rate of cleavage of carbon–carbon bonds involving secondary and primary carbon at-

TABLE 3

Isomerization of 2-Methylpentane on Iridium and on Iridium–Cobalt Catalysts (reduced 6 h at 973 K), T = 493 K

Catalyst	Weight, w (g)	α_T (mol%)	$r_T \times 10^3$[a]	S[b] (%)	$2C_3$	3MP[c]	nH	MCP	iP/nP	3MP/nH	$(C_2 + C_4)/(C_1 + C_5)$	Hydrogenolysis of methylcyclopentane	
												r = 3MP/nH	T (K)
Ir/Al_2O_3													
10% Ir[e]	0.25	45.8	66	10.5	12.5	9.4	0.8	0.3	3.3	11.7	1.3	48	433
0.5% Ir[e]	0.5	11	6	22.8	10.3	20.2	1.3	1.3	5	15.5	2.0	19	433
	0.5	25	12	19.3	10.5	16.1	2.2	1.0	3.4	7.2	2	—	
0.25% Ir[e]	1.6	3.8	0.15	21.8	5.8	13.4	4.7	3.7	2.5	2.8	2.5	—	
	1.6	30.9	1.5	23.2	7.8	16.8	3.8	2.6	2.2	4.4	2.3	16	433
1% Ir/SiO_2[d]	0.2	28.9	85	22.2	9.4	18.8	2.7	0.7	2.0	6.9	1.5	38	433
$Ir–Co/Al_2O_3$													
G	0.5	8.1	0.6	16.1	5.4	8.9	4.0	3.2	3.3	2.2	3.4	3.5	433
F	1	7	1	23.4	3.7	11.1	8.9	3.4	2	1.2	3.8	3.0	433
E	0.5	3.1	0.5	37.4	2.6	18.2	10.6	8.6	1.25	1.7	2.4	2.8	433
D	0.625	4.7	0.3	10.3	5.7	6.3	1.9	2.1	2	3.3	0.6	15.8	433
C	1	11.4	0.9	20.4	3.5	14.2	4.2	2.0	5	3.4	1.5	10.5	433
B	1	37.8	3	11.1	6.7	8.2	2.2	0.7	5	3.8	2.1	5.0	433
B*	0.5	16.1	9	26.8	15.9	18	2.5	1.0	2.3	7.2	1.4	20	433
Ib	0.2	1.3	1.6	28.2	3.0	19.3	5.2	3.7	5.8	3.7	5.2	5.9	453
Ia	0.2	3.5	4.3	10.6	5.4	6.9	2.3	1.4	1.2	31.6		6.7	473
Jb	0.2	6.1	7.5	28.5	4.6	21.3	4.6	2.6	2.3	4.6	3.4	9–15	453–473
Ja	0.2	7.8	5.1	12.1	2.7	6.1	5.0	1.0	3.8	1.2	4.9	4.6	453

[a] Total activity, $r_T \times 10^3 = (1 - \alpha_T)(F/w)\ln(1/(1 - \alpha_T))$ expressed in (μl g^{-1} s^{-1}) where α_T is the total conversion in mole percent, F is the hydrocarbon flow rate in μl s^{-1}, and w is the weight of catalyst in grams.

[b] Selectivity of isomers.

[c] 3MP, 3-methylpentane; nH, *n*-hexane; MCP, methylcyclopentane; iP, isopentane; nP, *n*-pentane; iB, isobutane; nB, *n*-butane.

[d] This catalyst was kindly supplied by Professor V. Ponec and used in his laboratory (*17*).

[e] These catalysts were prepared by the usual impregnation method already described in Ref. (*2*).

TABLE 4

Isomerization of 2-Methyl[2-C[13]]pentane on Iridium Catalysts at 493 K: Distribution of the Various Isotopic Species

Catalyst			[a]	% Cyclic mechanism			[a]	BSA[b] (%)
10% Ir–Al_2O_3	96	4	0	96	96	4	0	4
0.5% Ir–Al_2O_3	90	10	0	90	98	2	0	2
0.25% Ir–Al_2O_3	80	20	0	80	95.5	4.5	0	4.5
1% Ir–SiO_2	79.5	20.5	0	79.5	93	7	0	7

[a] Abnormal labeling corresponding to repetitive processes.
[b] Bond shift in chain lengthening.

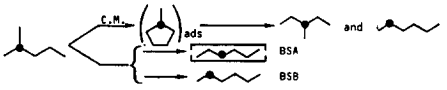

oms is 4 to 10 times higher than the rate for bonds involving a tertiary carbon atom. In Table 3 the ratio isopentane/*n*-pentane (iP/nP) varies from 2 to 5. In these experiments no repetitive process occurs: (i) extensive cracking does not take place, $6C_1 \sim 0$ and $3C_2 \sim 0$, except on the 0.25 wt% Ir/Al_2O_3 catalyst, (ii) the isobutane to *n*-butane ratio is always very high (iB/nB ~ 7), and (iii) the isomerized product distribution shows 7 to 15 times more 3-methylpentane than *n*-hexane.

To obtain deeper insight into the mechanism, the analytical technique was improved so that very small amounts of labeled *n*-hexane could be measured during isomerization of the labeled hydrocarbons.

The results presented in Tables 4 and 5 are different from those in Ref. (*2*) in which experiments with 2-methyl[4-^{13}C]pentane were not performed with as high a sensitivity as used in the analytical technique. From the relative contributions of *n*-hexane and 3-methylpentane, the amount of each isomer formed via the cyclic or bond-shift mechanism can be determined.

There are two main features: (i) the major isomerization pathway on iridium at low temperature (493 K) proceeds via the selective cyclic mechanism. (ii) Considering the

TABLE 5

Isomerization of 2-Methyl[4-^{13}C]pentane and 3-Methyl[3-^{13}C]pentane to *n*-hexane on Iridium Catalysts at 493 K: Distribution of the Various Isotopic Species

Catalyst	2-Methyl[4-^{13}C]pentane				3-Methyl[3-^{13}C]pentane			
			[a]	% Cyclic mechanism			[a]	% Cyclic mechanism
10% Ir–Al_2O_3	75	25	0	50	66	34	0	66
0.5% Ir–Al_2O_3	78.75	21.25	0	42.5	43	57	0	43
0.25% Ir–Al_2O_3	88	12	0	24	50	50	0	50
1% Ir–SiO_2	77	23	0	46	63.5	36.5	0	63.5

[a] Abnormal labeling corresponding to repetitive processes.

same isomer (e.g., *n*-hexane) the expected percentages obtained from 2-methyl[4-^{13}C]pentane or 3-methyl[3-^{13}C]pentane via the cyclic mechanism fully agree with the experimental findings.

The cyclic mechanism is three to seven times more effective than rearrangement via bond shift and represents 81 ± 7% of the isomer products as indicated in Table 6. The high (3-methylpentane/*n*-hexane)$_{CM}$ ratio indicates that the methylcyclopentane intermediates formed in the cyclic mechanism (CM) are hydrogenolyzed via a *very selective* pathway. Only the carbon–carbon bonds involving secondary carbon atoms are selectively broken.

Hydrogenolysis of methylcyclopentane performed at 433 K yielded almost exclusively 2-methylpentane and 3-methylpentane as seen in Table 3. The 3MP/nH ratio is always higher than 19 on all four Ir catalysts, which demonstrates that hydrogenolysis on iridium proceeds via the *selective mode*.

Catalytic behavior of iridium–cobalt catalysts. The results obtained with 2-methylpentane at 493 K are summarized in Table 3. The rate, r_T, expressed in μl (g s)$^{-1}$, is two to three orders of magnitude lower for catalysts B to G than for the monometallic catalysts with 1 or 10 wt% Ir. On the other hand, the catalysts in the second series (Ia, Ib, Ja, Jb) are 2 to 20 times more active than catalysts F and D, respectively. No large variation in r_T values occurs when the Ir content changes from 0.3 to 6 wt% metal loading. They are comparable to those obtained on the 0.25 wt% Ir/Al_2O_3 catalyst.

Besides isomerization, hydrogenolysis is again the most important reaction. No multiple C–C bond cleavage occurs, which is quite surprising with respect to the properties of cobalt catalysts (*18*). $6C_1 \sim 0$ and $3C_2 \sim 0$ and iB/nB > 7, except catalyst J_a (3.9 wt% iridium) for which an important fraction of $3C_2$ is produced.

The $C_4 + C_2/C_1 + C_5$ ratio depends on catalyst composition and passes through a minimum for the coimpregnated series. As on iridium catalysts, C–C bond rupture involving a tertiary carbon atom is not favored; the iP/nP ratio is higher than 1.2.

The selectivity in C_6 isomer formation changes with catalyst composition. A maximum value of 37.4% is reached for catalyst E (1.9 wt% Ir) and a minimum for catalyst D (3.9 wt% Ir). For the catalysts in the second series, where cobalt is second in the sequence of impregnation, the selectivity is around 10% compared with the 28% characteristic of the catalyst where the support is impregnated first with cobalt. The 3MP/nH ratio changes from 2.2 for catalyst G to 3.8 for B, passing through a minimum of 1.2 indicative of catalyst F. This ratio varies erratically in the second series but the values fall in the same range. As on pure iridium catalysts, the amount of methylcyclopentane is near that of *n*-hexane.

On the other hand, in methylcyclopentane hydrogenolysis, the 3MP/nH ratio is always high and comparable to that obtained on Pt/Al_2O_3 catalysts with large particles, but r is lower on monometallic iridium catalysts (see Table 3). The values depend on catalyst composition: at 433 K, from 0.3 to 1.9 wt% Ir, $r = 3.1 \pm 0.4$; from 3.9 to 6 wt% Ir, $r = 13.5 \pm 3$; and for 7.7 wt% Ir, $r = 5$.

For catalysts in the second series, the experiments were performed at various temperatures; the results obtained are in the same range as those previously obtained.

In the isomerization of labeled hydrocarbons, the ratio of cyclic to bond-shift mechanism is only 1 to 3 as shown in Table 6. This behavior is typical of Ir–Co catalysts.

Addition of iridium to cobalt also resulted in a decrease in the contribution of the cyclic mechanism and in the 3MP/nH ratio obtained either by methylcyclopentane hydrogenolysis or during hydrogenolysis of the cyclic intermediate (3MP/nH)$_{CM}$.

For catalyst B* treated under helium at 1273 K the product distributions for both isomerization and hydrogenolysis are characteristic of a monometallic iridium on alumina catalyst (Table 3).

TABLE 6

Distribution of the Various Mechanisms at 493 K on Ir and on Ir–Co Catalysts (from 100 mol of 2-Methylpentane)

Catalyst		Conversion α_T[a] (mol%)	$\Sigma_{cracking}$	Σ_{BS}	Σ_{CM}	$\frac{nH_{BSA}}{\Sigma_{BS}} \cdot 100$ (%)	Σ_{CM}/Σ_{BS}	$\frac{\Sigma_{CM}}{\Sigma_{BS}+\Sigma_{CM}} \cdot 100$	$(3MP/nH)_{CM}$
10% $Ir-Al_2O_3$		45.8	41	0.6	4.2	0.75	7	87.5	21
0.5% $Ir-Al_2O_3$		11	8.5	0.3	2.2	0.55	7.3	88	33
0.25% $Ir-Al_2O_3$		3.8	3	0.2	0.6	2.5	3	75	9.7
1% $Ir-SiO_2$		28.9	22.5	1.5	4.8	1.95	3.2	76	12
Ir (at%)	Co (at%)								
1	99	8.1	6.8	0.4	0.8	2	2	66	4.6
2	98	7	5.3	0.8	0.8	1.9	1	50	5.3
7	93	3.1	1.9	0.4	0.7	1.75	1.75	63.5	3.6
16	84	4.7	4.2	0.2	0.3	11	1.5	60	5.5
32	68	11.4	9	0.5	1.7	3.6	3.4	77	7
50	50	37.8	33.6	1.3	2.9	2.8	2.2	69	9.5

[a] $\alpha_T = \Sigma_{cracking} + \Sigma_{BS} + \Sigma_{CM}$; $\Sigma_{cracking}$ = amount of molecules formed by cracking reactions; $\Sigma_{BS} + \Sigma_{CM}$ = amount of molecules formed by bond-shift mechanisms and cyclic mechanisms. nH_{BSA} = amount of *n*-hexane formed by bond-shift A.

DISCUSSION

Supported Iridium Catalysts

In light of the isomerization properties observed for iridium catalysts, first the relationship between selectivity and particle size is discussed. Skeletal rearrangement of hydrocarbons on various crystallographic planes of iridium is as structure sensitive as on platinum surfaces (*19*). Nevertheless, clear evidence, as was shown on Pt (*4*), regarding the particle size effect on hydrocarbon reactions on iridium is not available here. Van Santen *et al.* (*17*) studied the role of surface carbonaceous layers and of metal particle size in the reactions of C_6 hydrocarbons. They concluded that (i) methylcyclopentane ring opening is selective on clean iridium (no hexane is formed), and when iridium is covered with a carbonaceous layer, less selective ring opening occurs; (ii) the dependence of particle size on the catalytic properties of Ir, as well as its sensitivity to self-poisoning, is much less pronounced than on Pt.

As far as our results are concerned, with decreasing iridium concentration the relative contribution of *n*-hexane in the isomerization of 2-methylpentane increases, but this is not related to nonselective hydrogenolysis of the methylcyclopentane ring, as shown in Table 3. Nor can this be ascribed to formation of a carbonaceous deposit, because no repetitive processes occur, as indicated by the distribution of labeled isomerized products shown in Tables 4 and 5 (no abnormal labeling can be detected by [1-^{13}C]hexane or 3-[methyl^{13}C]pentane formation).

The relative contribution of the cyclic mechanism decreases when the metal loading decreases, as shown in Table 6, which demonstrates very clearly that iridium and platinum behave very differently. To explain this behavior the following experimental findings should be taken into consideration: (i) when the cyclic contribution is equal to 75% ($\Sigma_{CM}/\Sigma_{BS} = 3$), bond shift via mode A (BSA) occurs to a higher extent; (ii) hydrogenolysis of the methylcyclopentane intermediate is always selective; (iii) in the isomerization of 2-methylpentane,

$(3MP/nH)_{CM}$ decreases significantly from 33 to 9.7 as iridium content decreases.

For interpretation of these results a property of metal particles associated with small size should be utilized. Indeed, iridium atoms in small particles may behave as in organometallic entities and it is well known that on iridium a carbyne structure is favored. Here, reaction schemes involving alkyne species for bond-shift A isomerization [reaction (1)] and for interpretation of the high isopentane/*n*-pentane ratio [reaction (2)] are suggested:

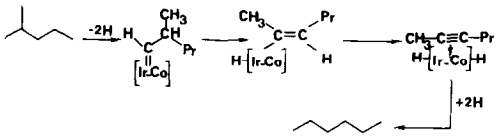

(1)

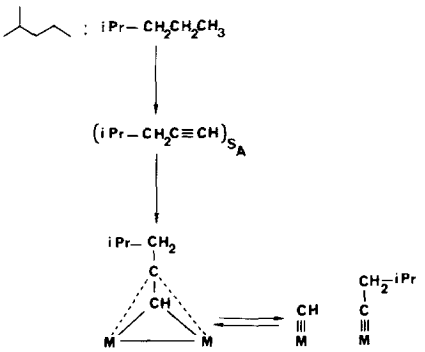

dehydrogenation on the adsorption sites S_A (*25*)

superficial migration to reactive sites S_R (*25*) composed of metals with low coordination numbers, noted "M≡M" (*26, 27*) (2)

However, influence of the support, which is more important when the particle sizes are smaller or when the support is different (Al_2O_3 or SiO_2), cannot be ruled out. On the basis of this new evidence obtained on various supported iridium catalysts, our previous proposal for 1,3 methyl shift mechanism (*2*) should be omitted.

Iridium–Cobalt Catalysts

Concerning the isomerization of 2-methylpentane, it is observed that the iridium–cobalt samples are less active than the monometallic 10 wt% Ir/Al_2O_3 catalyst. Surprisingly, however, these bimetallic iridium–cobalt catalysts are as active as the 0.25 wt% Ir/Al_2O_3 catalyst, whatever the dilution of iridium to cobalt. Furthermore, the isomer selectivity is characteristic of monometallic iridium catalyst and not of cobalt. On $Ir_{50}Co_{50}/Al_2O_3$ (catalyst B*) composed of fcc Ir particles (see EXAFS results, Table 2) the selectivity is similar to that measured on the 10% Ir/Al_2O_3 sample. When iridium atoms are located on the topmost layer the selectivity resembles those obtained on catalysts with low Ir loading (0.5 and 0.25 wt% Ir/Al_2O_3). On monometallic cobalt catalysts the selectivity for isomerization is zero at 493 K (*18*). Hence, from the data it can be concluded that association of cobalt with iridium always results in an iridium character, even for a very high dilution of iridium in cobalt (1 or 2 at% iridium for 99 or 98 at% cobalt, respectively).

Further support for the display of iridium characteristics of the Ir–Co bimetallic systems is derived from the increased selectivity of isomerization observed on catalysts Ib and Jb, when cobalt salts are first impregnated. These findings seem not too surprising when the structure of Ir–Co cata-

lysts is considered in light of the EXAFS measurements (see Table 2). The surface is always covered with iridium and the surface composition in iridium seems constant. A higher content of iridium results in the same surface composition and in enhancement in the bulk (small contracted iridium clusters). In addition, TPR measurements (*7*) completely support the EXAFS data.

Another important feature emerges from the product distribution of methylcyclopentane hydrogenolysis. At such temperatures, the selectivity in C_6 isomers amounts to about 100% both on monometallic iridium and on bimetallic iridium–cobalt catalysts. Again, this is completely different from the behavior of a cobalt catalyst (*18*) where C_6 isomer selectivity equals zero. Furthermore, the 3MP/*n*-hexane ratio deviates noticeably from that measured over monometallic iridium catalysts, with the exception of sample D (Co 84.8–Ir 15.2) for which the 3MP/nH ratio reaches $\simeq$16 due to the presence of Ir particles (Ir–Ir = 0.272 nm) as detected by EXAFS. However, it is worthwhile to recall that some metal–support interaction may occur on a catalyst with low iridium loading as shown in the previous paragraph. Consequently, here again the bimetallic Ir_xCo_{1-x} catalysts reflect large differences from monometallic cobalt or iridium catalysts. No direct correlation with a linear combination of properties of cobalt or iridium is possible. At this point one may think that dilution of iridium by cobalt will result in an increase in the nonselective hydrogenolysis of MCP as observed on Pt–Cu catalysts (*20*) or Ir–Cu catalysts (*15*).

Results of the labeling experiments, in particular the ratios presented in columns 6–8 in Table 6 for Ir_xCo_{1-x}/Al_2O_3 samples and for the monometallic iridium catalysts, are evidence that the bimetallic catalysts have gained different characteristics toward isomerization compared with iridium catalysts, even if a support effect is operative for monometallic iridium catalysts.

In contrast to the properties of platinum displayed in the copper-diluted samples (*20*) or in the very small Pt particles, here an increase in both the nonselective pathway in hydrogenolysis of methylcyclopentane and in the contribution of the bond-shift mechanism to skeletal rearrangement is induced by dilution of iridium with cobalt. The same trends were observed recently for bimetallic Pt_xCo_{1-x}/Al_2O_3 and Ir_xCu_{1-x}/Al_2O_3 catalysts (*5, 6, 21*).

Both the particle size effect and the dilution of Ir by Co indicate the importance of participation of carbyne-type intermediates in the rearrangement. These carbyne species of Ir and Co (*22, 23*) can be synthesized and under certain conditions can be stabilized on the support. The observed changes do not contradict its being an intermediate; therefore, the presence of alkyne-adsorbed species as intermediates for the skeletal rearrangement of hydrocarbons on bimetallic iridium cobalt catalysts can be postulated. Cleavage of these alkyne species produces surface carbynes (*6*).

As an alternative explanation one may assume the depletion of surface hydrogen as cobalt increases. Guczi *et al.* (*7*) have shown for carbon monoxide hydrogenation on $Co–Ir/Al_2O_3$ bimetallic catalysts that there is a proportionality between CH_4 formation and the easily available, weakly bound hydrogen. TPD experiments showed that addition of cobalt to iridium resulted in a change in the proportion of hydrogen desorbed at low temperature (on iridium) to that characteristic of cobalt samples desorbed at higher temperature. This latter is not strongly bound to the surface for the hydrogenation step in any surface reaction; as a consequence, the larger the amount of strongly bonded hydrogen on the surface, the higher the proportion of alkyne species formed and, hence, the contribution of selective cyclic mechanism decreases.

CONCLUSIONS

Catalytic properties of iridium catalysts clearly show that the selective cyclic mechanism predominates. When the total metal loading decreases the relative contribution

of the cyclic mechanism decreases, whereas the bond shift in the chain lengthening via mode A (methyl migration) increases. We proposed that among the parallel reactions occurring, the selective cyclic mechanism is weakened and alkyne species formation is favored.

No discrepancy exists between the percentages obtained from 2-methyl[4-^{13}C]pentane and 3-methyl[3-^{13}C]pentane via the cyclic mechanism when looking at *n*-hexane formation. These results seem to rule out the previous proposal for a 1,3 methyl shift mechanism (*2*). Furthermore, the weak influence of the support seems to contribute when the support is different (Al_2O_3 or SiO_2) and the total amount of iridium decreased.

The cyclic mechanism is always the major process on iridium–cobalt catalysts but its role is lower than on pure iridium. On the other hand, the role of the bond-shift A mechanism is increased and the $(3MP/nH)_{CM}$ ratio is decreased.

Two phenomena are operative on these catalysts. First, to explain the nonreactivity of tertiary carbon atoms and all the results above, we may postulate an alkyne mechanism which produces, by cleavage, surface carbynes. Second, as there is a large excess of hydrogen, to explain a dehydrogenation to alkyne species we must view it as a result of the lesser availability of surface hydrogen since as cobalt increases the weakly bound surface hydrogen diminishes.

Finally, we may note that the catalytic behavior of cobalt is never reached. This means that an interaction between Ir and Co blocks the extensive cracking properties of cobalt. These results are very well explained by the EXAFS measurements which indicate that the surface composition in iridium is constant, whatever the iridium loading, with iridium atoms surrounded only by cobalt atoms.

ACKNOWLEDGMENT

The authors are grateful to Dr. M. Guenin, Institut de Recherches sur la Catalyse, Villeurbanne, France, who analyzed the catalyst with 0.25% Ir by TEM.

REFERENCES

1. Weisang, F., and Gault, F. G., *J. Chem. Soc. Chem. Commun.*, 519 (1979).
2. Garin, F., Girard, P., Weisang, F., and Maire, G., *J. Catal.* **70,** 215 (1981).
3. Fritsch, A., Thesis, Université Louis Pasteur, Strasbourg, 1987.
4. Dartigues, J. M., Chambellan, A., Corolleur, S., Gault, F. G., Renouprez, A., Moraweck, B., Bosch-Giral, P., and Dalmaï-Imelik, G., *Nouv. J. Chim.* **3,** 591 (1979).
5. Zyade, S., Garin, F., Hilaire, L., Ravet, M. F., and Maire, G., *Bull. Soc. Chim. Fr.* **3,** 341 (1985).
6. Zyade, S., Garin, F., and Maire, G., *Nouv. J. Chim.* **11,** 429 (1987).
7. Guczi, L., Matusek, K., Bogyay, I., Garin, F., Esteban Pugès, P., Girard, P., and Maire, G., *C_1 Mol. Chem.* **1,** 355 (1986).
8. Corolleur, C., Corolleur, S., and Gault, F. G., *J. Catal.* **24,** 406 (1972).
9. Garin, F., and Gault, F. G., *J. Amer. Chem. Soc.* **97,** 4466 (1975).
10. Lagarde, P., Murata, T., Vlaic, G., Freund, E., Dexpert, H., and Bournonville, J. P., *J. Catal.* **84,** 333 (1983).
11. EXAFS Soft. Georgiopoulos and S. Knapp, (GSK Inc.)
12. Teo, B. K., and Lee, P. A., *J. Amer. Chem. Soc.* **101,** 2815 (1979).
13. Hansen, M., "Constitution of Binary Alloys," Metallurgy and Metallurgical Engineering Series. McGraw–Hill, New York, 1958.
14. Apai, G., Hamilton, J. F., Stohr, J., and Thompson, A., *Phys. Rev. Lett.* **43,** 165 (1979).
15. Maire, G., Bernhardt, P., Garin, F., Girard, P., Schmitt, J. L., Dartyge, E., Dexpert, H., Fontaine, A., Jucha, A., and Lagarde, P., *Appl. Catal.* **26,** 305 (1986).
16. Maire, G., and Garin, F., *in* "Catalysis: Science and Technology" (J. R. Anderson and M. Boudart, Eds.), Vol. 6, p. 162. Springer-Verlag, Berlin, 1984.
17. Van Santen, J. G., Van Broekhoven, E. H., Wreesman, C. T. J., and Ponec, V., *J. Catal.* **87,** 468 (1984).
18. Zyade, S., Thesis, Université de Strasbourg, 1984.
19. Witt, J., and Nieuwenhuys, B. E., *Surf. Sci.* **119,** 1 (1982).
20. de Jongste, H. C., Ponec, V., and Gault, F. G., *J. Catal.* **63,** 395 (1980).
21. Sárkány, A., Garin, F., Petit, C., and Maire, G., to be published.
22. Parshall, G. W., Thorn, D. I., and Tulip, T. H., *Chem. Technol.*, 571 (1982).
23. Fritch, J. R., and Vollhardt, K. P. C., *Angew. Chem. Int. Ed. Engl.* **19,** 559 (1980).
24. Gault, F. G., Zahraa, O., Dartigues, J. M., Maire, G., Peyrot, M., Weisang, E., and Engelhard, P. A., *in* "Proceedings, 7th International Congress

on Catalysis (Tokyo, 1980)," Vol. 1, p. 199. Kodansha/Elsevier, Tokyo/Amsterdam, 1981.
25. Dauscher, A., Garin, F., and Maire, G., *J. Catal.* **105,** 233 (1987).
26. Chisholm, M. H., Folting, K., Hoffman, D. M., and Huffman, J. C., *J. Amer. Chem. Soc.* **106,** 6794 (1984).
27. Listemann, M. L., and Schrock, R. R., *Organometallics* **4,** 74 (1985).
28. Majerus, J., Petit, C., Esteban, P., Maire, G., Dartyge, E., Dexpert, H., and Tourillon, G., LURE report for 1987, to be published.
29. Weisang, F., Thesis, Université de Strasbourg, (1979); F. Weisang and F. G. Gault (unpublished results).
30. Esteban, P., Majerus, J., Maire, G., Dartyge, E., and Dexpert, H., *J. Phys. Chem.*, in press.